Holographic fabrication of photonic nanostructures for optofluidic integration

Seung-Kon Lee,†[a] Sung-Gyu Park,†[a] Jun Hyuk Moon[b] and Seung-Man Yang*[a]

Received 20th November 2007, Accepted 2nd January 2008
First published as an Advance Article on the web 9th January 2008
DOI: 10.1039/b717960j

Holographic lithography in combination with photo-lithography provides a novel optofluidic platform through incorporation of periodic photonic units inside the microfluidic chips in a highly compatible and facile way.

Recently, various periodic photonic nanostructures made of dielectric materials or metals have been studied extensively due mainly to their potential characteristics for high efficiency photonic devices and sensors. Electromagnetic waves striking into the periodic nanostructures have specific interactions which lead to various photonic properties such as photonic band-gaps (PBG), localized surface plasmon resonance (LSPR) and surface enhanced Raman scattering (SERS).[1–3]

In particular, optofluidics is a rapidly emerging technology to increase the potential capabilities of optics/photonics and microfluidics by incorporating photonic nanostructures inside microfluidic devices. In optofluidic systems, fluidics gives adaptive, addressable and tunable capability to photonic devices while photonics reduces response time drastically and provides rapid *in-situ* sensing of analytes.[4] The characteristics of photonic devices can be finely tuned in microfluidic systems, because the interaction between light and photonic structures varies sensitively with the change in refractive index of the medium.[5,6] Consequently, photonic structures which are built in microfluidic channels are an ideal platform for lab-on-a-chip or micro-TAS devices which require real-time analysis of infinitesimal amounts of chemicals and biological substances.[7]

Recently, a number of researches have been conducted to integrate periodic photonic nanostructures within desired sites of microfluidic devices. Several clever ways including electron beam lithography, soft-lithography and colloidal self-assembly have been developed to incorporate 2D and 3D functional nanostructures exhibiting PBG or SPR/SERS inside microfluidic chips.[8–10] However, these approaches either produce undesired defects or require complex processes as well as highly expensive advanced lithographic equipment for rapid fabrication of integrated optofluidic chips. Also, although direct laser writing or block copolymer self-assembly is useful to achieve 3D periodic structures, these alternatives cannot incorporate readily 3D structures in confined microfluidic chips.

[a]*National CRI Center for Integrated Optofluidic Systems and Department of Chemical and Biomolecular Engineering, Korea Advanced Institute of Science and Technology, 305-701, Deajeon, Korea. E-mail: smyang@kaist.ac.kr*
[b]*Samsung Advanced Institute of Technology, Gyeonggi-Do, 446-712, Korea*
† These authors contributed equally to this project.

Meanwhile, holographic lithography (HL) has great potential for simple and rapid production of 2D and 3D defect-free ordered structures with submicrometer scale periodicity over large areas. In HL, multi-beam interference produces a multi-dimensional intensity profile of light in space. The interference-induced intensity profile can be transferred to photopolymerizable resins in very short exposure times ranging from a few nanoseconds to seconds.[11] More importantly, HL allows for precise control of the feature size and shape of the resulting structures with flexibility to access a variety of lattice symmetries through a proper arrangement of laser beams. However, conventional HL setups use a number of optical components such as beam splitters, mirrors and polarizers and require sophisticated procedures for beam alignment and reconfiguration. Recently, Wu *et al.* proposed a novel refracting prism HL, which makes the bulky complicated system simple as well as removes difficulty in beam alignment.[12] Nevertheless, tunability of optical properties of as-fabricated structures are still limited and remain a challenging issue in this field.[13]

In this communication, we present a simple method for fabricating optofluidic chips of which microfluidic parts are formed by photo-lithography and photonic substrates are built in by the single prism HL. In fact, this is the first report on the combination of HL and photo-lithography for optofluidic integration. For optofluidic integration, HL has several unique advantages over other methods for periodic nanostructures. For example, HL is compatible with conventional photo-lithography because both techniques use similar photo-chemistry for fabricating designed structures in polymers. In our optofluidic systems, 3D structures featured by HL have PBGs due to their structural periodicity while microfluidic flows of liquids with different refractive indices can tune the PBGs. The modulation of the PBGs for various liquid flows is confirmed by changes in the intensity and peak position of the reflectance spectra in IR region. In addition, the built-in periodic structures in microfluidic devices by HL have multi-dimensional interconnected open pores, which provide large surface areas for catalytic reactions, biological adsorption and kinematic fluid mixing.[14–16]

The materials used in HL and photo-lithography experiments were epoxy-based resin (EPON SU-8, Resolution Performance Product) and 1–2 wt% of photoacid generator (Cyracure UVI-6992, Dow Chemical), both dissolved in GBL (γ-butyrolactone, Sigma-Aldrich). The photoresist (PR) film of 300 nm–10 μm in thickness was obtained by spin casting the solution on a glass substrate and subsequent softbaking at 95 °C to evaporate the solvent. Then, laser was exposed to the PR for 0.1–1 s. A proper exposure condition was determined by the photoinitiator content and the PR film thickness.

After the post-exposure baking process, unexposed regions were removed by PGMEA (propylene glycol methyl ether acetate, Sigma-Aldrich) during development. Rinsing with 2-propanol left behind highly polymerized regions by UV exposure. For 2D structures, a positive PR (AZ 5214, Shipley) was used alternatively. UV-cured SU-8 has sufficient mechanical strength for microfluidic operations and the surface properties can be modified by acid treatment for chemical or biological applications.[17]

The optical setup for the 2D and 3D HL is schematically illustrated in Fig. 1a. The laser beam (He–Cd laser, CW, 325 nm, 50 mW, Kimmon) is expanded by 10 times through the beam expander and then impinges perpendicularly to the top-cut fused silica prism whose refractive index is 1.48 at the wavelength of 325 nm. The geometric feature of the prism is shown in Fig. 1b. As noted, three beams designated by wave vectors, $\boldsymbol{k}_1$, $\boldsymbol{k}_2$, and $\boldsymbol{k}_3$ are generated by refraction from three side surfaces of the prism and another beam of wave vector $\boldsymbol{k}_0$ travels through the top surface of the prism. The four different beams are recombined at the bottom surface in which an interference pattern is created.

The resulting multi-dimensional interference pattern is transferred latently in the SU-8 photosensitive prepolymer resin and activates polymerization.

The holographic intensity profile I can be expressed by the general interference equation:

$$I = \sum_i \vec{E}^2 + \sum_{i<j} \vec{E}_i \cdot \vec{E}_j \cos\left[(\vec{k}_i - \vec{k}_j)\cdot\vec{r} + (\varphi_i - \varphi_j)\right] \qquad (1)$$

with wave vectors $\boldsymbol{k}_i = 2\pi/\lambda\ (\cos\beta_i \sin\alpha,\ \sin\beta_i \sin\alpha,\ \cos\alpha)$ derived from Snell's law for the prism of cutting angle of 54.7°. Here, λ is the wavelength of the laser, and α and β_i are the polar and azimuthal angle of $\boldsymbol{k}_i$ as shown in Fig. 1b. Therefore, the intensity profile I of the resulting interference pattern can be determined by the electric fields $\boldsymbol{E}_i$, wave-vectors $\boldsymbol{k}_i$ and phase shifts ϕ_i.[18] Fig. 1c shows 2D and 3D interference patterns that were simulated from eqn (1). A 3D graphic software was used to calculate the isointensity surface of multi-dimensional interference profiles. 2D and 3D structures can be controlled by adjusting the thickness of the PR layer with the given prism.

In order to integrate as-fabricated holographic nanostructures into micropatterns such as microfluidic channels, an additional photo-lithography step is used before or after the HL step. As shown in the experimental scheme of Fig. 1d (i)–(iii), HL and photo-lithography were employed simultaneously to pattern 2D and 3D photonic crystal structures within pre-patterned microstructures. In the photo-lithography step, the PR film was exposed through predesigned photomasks by 365 nm UV light from the Hg arc lamp mounted on a mask aligner. It should be noted that the PR materials used here were compatibly responsive to both a 325 nm He–Cd laser source and a 365 nm Hg lamp source. At this point, three different regions are formed in the PR; unexposed areas, the regions exposed solely by the interference pattern but shaded from the photo-lithography source, and the areas which were exposed twice by both HL and photo-lithography sources according

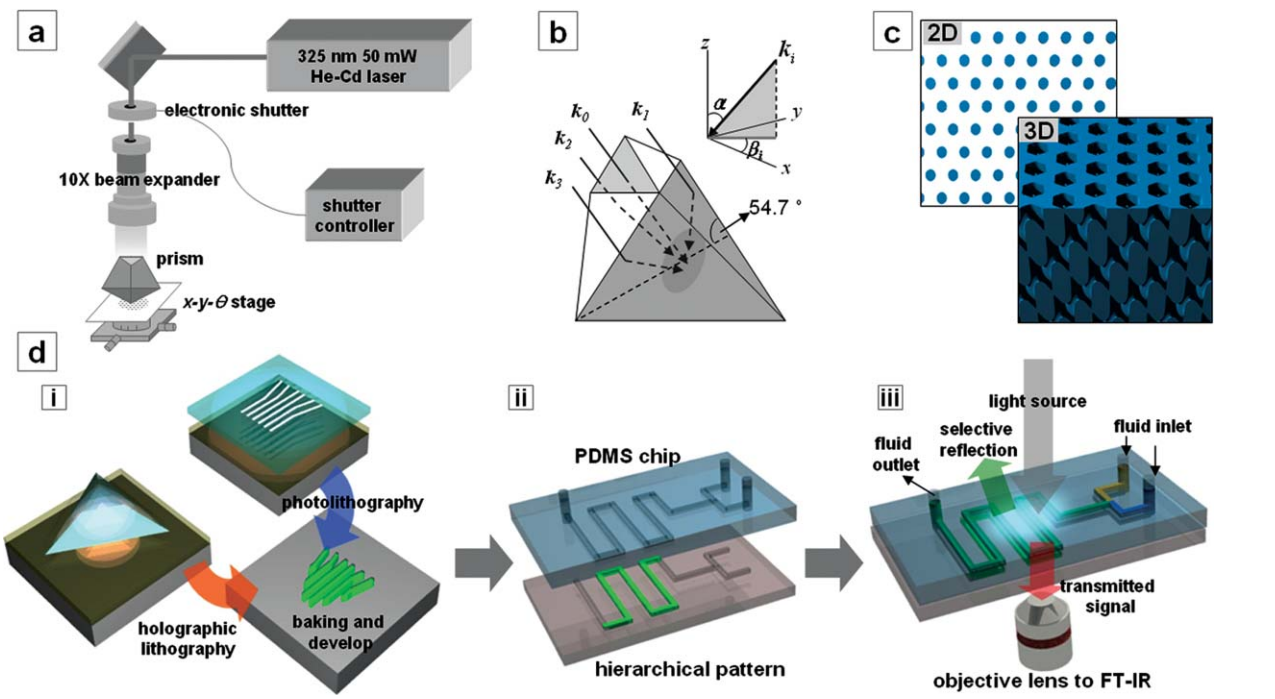

Fig. 1 Schematics of experimental setup, procedure and beam arrangement for optofluidic integration. (a) Optical setup for prism HL. The 325 nm He–Cd laser beam was expanded by a beam expander and split and recombined at the stage. The exposure time was controlled by an electronic shutter and controller. (b) Geometry of the prism and resulting wave-vectors from top-cut prism with a 54.7 ° corner angle. $\boldsymbol{k}_0$ came through the top surface and $\boldsymbol{k}_1$–$\boldsymbol{k}_3$ were refracted from slanted side planes. These four beams were recombined at the bottom surface of the prism. (c) 2D and 3D simulation images of multi-beam interference patterns with given wave vectors. (d) Schematic procedure of optofluidic chip fabrication: (i) combination of HL and photo-lithography for hierarchical pattern formation, (ii) integration of HL-featured photonic structures with microfluidic chip, (iii) illustrative optofluidic system for real-time characterization of optical spectra. Here, incident light was selectively transmitted by periodic nanostructures and collected by an objected lens to transfer the optical signal to a FT-IR spectrometer. Optical signals were analyzed with varying the refractive index of the injected fluids.

to the shape of the photomasks. The unexposed parts were removed from the PR film using the developer, which left behind hierarchically patterned micro/nanostructures. Then, for optofluidic integration of the photonic crystal patterns within the microfluidic device, the PDMS microfluidic chip was combined with as-prepared hierarchical patterns. The PDMS microfluidic chip and SU-8 patterns were bonded together after oxygen plasma treatment of two facing sides. The combined chips were then annealed at 70 °C in a convection oven for 1 h to ensure the chemical bonding. This completes the fabrication of an integrated optofluidic device with built-in 2D/3D photonic crystals as shown in panel (iii) of Fig. 1d.

Fig. 2a shows the optical microscope image of a patterned sample which has holographic nanostructures within electronic chip micropatterns. Here, a 350 nm-thick positive PR was used to make a 2D nanostructure. The periodic nanostructure diffracted ambient light strongly showing a vivid violet color for a specific viewing angle. Basically, low magnification images beyond a certain resolution limit cannot display the featured nanostructures. However, if there is periodicity within their structures, Moiré fringes may appear by superposition of periodic structures and pixels of an imaging tool.[19] By using conventional sputtering or a dry-etching process such as reactive ion etching and ion milling, nanodot or nanohole patterns can be prepared for SPR or SERS substrate.[20] Fig. 2b is the scanning electron micrograph of hierarchical patterns in Fig 2a. Slanted stripes of Moiré fringe confirm the existence of periodic structures within the micropatterns. The inset in Fig. 2b shows a magnified view of hexagonally arrayed PR pattern coated with a 45 nm thick gold layer.

To incorporate a 3D nanostructure in the microfluidic channel, a 10 μm thick SU-8 film and a Y-shape photomask were used. Fig. 2c shows the resulting 3D structures built in the microfluidic channel. Also included in the insets of Fig. 2c are the magnified SEM images of the boundary and the surface morphology of HL-featured 3D ordered pore structures. The structure fabricated by HL with a prism has a face-centered cubic (fcc) symmetry of pore arrangement. The facing top surface of the structure is the [111] plane of fcc lattices as denoted by A, B and C. This periodic and interconnected pore structure inside of the microfluidic channels can be used for catalytic microreactors, passive type microfluidic mixers and filters as well as tunable optofluidic components.

In Fig. 2d, the cross-sectional image of the Y-shape pattern with a magnified view in the inset reveals that the unit atom of fcc lattices is elongated to the [111] direction and its interlayer distance is about 0.75 μm. The resulting 2D and 3D structures were in good agreement with the simulated interference patterns.

The periodic nanostructures have useful optical properties such as PBG, SPR and SERS, and they can be modulated sensitively in response to the optical properties of the surrounding medium. Therefore, the optical/photonic properties of the built-in nanostructures can be tuned instantly by infiltrating various fluids which have different refractive indices. Microfluidics enables one to use and manipulate infinitesimally small amount of samples for optical analysis, which is of potential significance in chemical or biological sensors and micro-TAS. On the other hand, the microfluidic modulation of PBGs of the built-in photonic crystals is essential for constructing PBG-based optofluidic platforms, which require fluidic addressability and adaptive controllability. Therefore, optofluidic chips with built-in photonic crystals have potential applications in active photonic devices such as waveguides, adaptable optical filters and switches and tunable microlasers.

As an illustrative purpose, we demonstrate the modulation of PBG in response to the change in the refractive indices of the flowing media. It is well known that the photonic crystals of fcc symmetry have a pseudogap (or so-called L-gap) for light propagating in the [111] direction.[21] The L-gap of fcc symmetry can be characterized by reflectance or transmittance spectra for normal incident light onto the [111] plane as shown in Fig. 3a. The location of reflectance peak can be expressed by Bragg's law:

$$\lambda = 2n_e d\sin\theta \tag{2}$$

in which λ is the peak wavelength of reflectance, d is the interlayer distance in the [111] direction and θ is the incident angle to the [111] plane. The effective refractive index n_e is simply estimated by following equation:

$$n_e = \sqrt{f n_f^2 + (1-f)\cdot n^2} \tag{3}$$

Here, n_f and n represent the refractive indices of the skeleton material of photonic crystal (*i.e.*, SU-8) and the flowing liquid, respectively, and f is the filling fraction of the structure. In our experiment, the reflection spectra of the HL-featured 3D

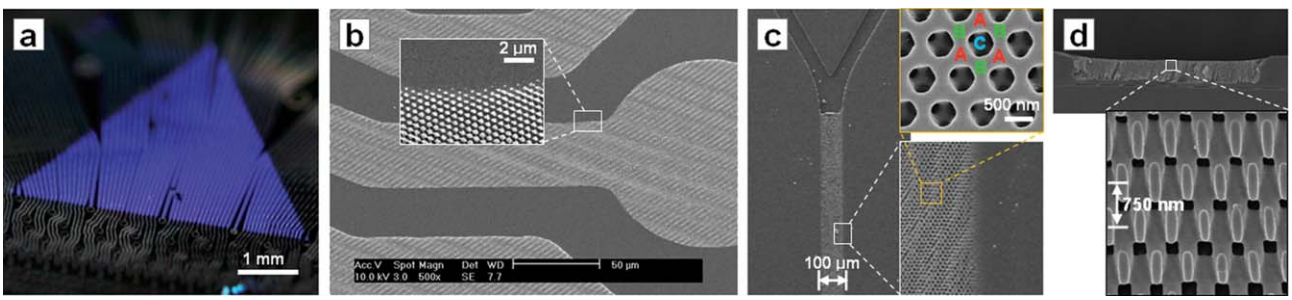

Fig. 2 Optical and scanning electron microscope (SEM) images of the resulting multi-dimensional micro/nanostructures. (a) Vivid violet color diffracted from the triangular part which has periodic nanostructures fabricated by holographic lithography within the electronic chip patterns. (b) SEM image of the hierarchical structure in panel (a). Scale bar is 50 μm. The inset shows a magnified view of the patterned periodic structure. (c) 3D nanostructures patterned in Y-shape microfluidic channels. The boundary between the porous nanostructures and the channel wall can be seen in the lower inset. The upper inset shows a magnified image of the 3D nanostructure with fcc symmetry. A, B and C represent the three repeated stacking layers of the fcc structure. (d) Cross-sectional image of the Y-shape channel. From the inset figure, the interlayer distance is 0.75 μm.

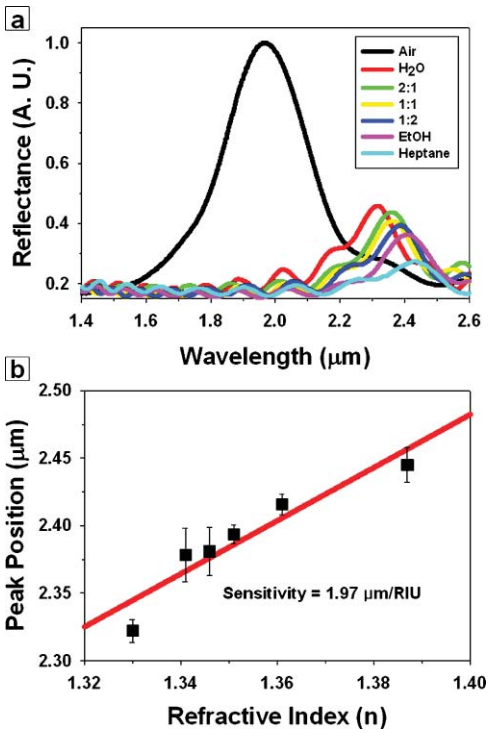

Fig. 3 Reflectance spectra and bandgap shifts of as-prepared optofluidic chip. (a) Reflectance spectra of the optofluidic chip with a 3D photonic crystal structure. The reflectance peak was tuned by refractive index mismatch between SU-8 and flow medium. (b) Linear tendency of peak-shift in response to the refractive index variation.

photonic crystals in the microfluidic channel were characterized by a FT-IR spectrometer (Bruker IFS 66 V/S) combined with an IR microscope (Hyperion 3000, Nikon). We used various pure and mixture liquids with different refractive indices including Air = 1, H_2O = 1.33, EtOH = 1.361 and heptane = 1.387. The mixtures of water and ethanol were prepared with three different mixing ratios 2 : 1, 1 : 1 and 1 : 2. Fig. 3a shows that the SU-8 photonic crystal structure in air displays a reflection peak at 1.97 μm for the incident light in the [111] direction. However, when the flowing medium is changed from air to higher refractive index liquids, the reflection spectra are modulated and red-shifted continuously. In the PDMS microfluidic channel, the liquids were filled into the 3D photonic nanostructures under the action of capillary forces and it took less than a few seconds for complete filling. It should be noted that fluctuation of the peak shift in response to the variation of fluid velocity was negligible for the volumetric flow rate ranging from 10 μL h^{-1} to 400 μL h^{-1}.

The filling fraction of the structure f can be calculated from Bragg's eqn (2) together with eqn (3). Using d = 0.75 μm (as measured from the SEM image) and n = 1.575 of SU-8, the PR filling fraction was 49%. By controlling the laser dose during the HL step, the filling fraction can be adjusted. With variation of the filling ratio, the range of wavelength exhibiting reflectance spectra can be controlled precisely as described in eqn (2) and (3). In Fig. 3b, the sensitivity of the PBG modulation was illustrated by plotting the peak shift as a function of the refractive index of the flow medium. The resulting peak shift in response to the variation of refractive index from pure water to heptane (n= 1.33–1.387) was as large as 1.97 μm per unit variation of refractive index, which is quite sensitive compared with the values of conventional SPR based sensors.[22]

In this communication, we report a simple and direct fabrication method for a novel optofluidic platform which has built-in nanophotonic structures within microfluidic chips. It is the first attempt to combine HL and photo-lithography for optofluidic integration. Since the presented method is based on a similar photochemical process, hierarchical patterns can be generated in a highly compatible way by simply adding a single exposure step to the conventional photo-lithography process. In this scheme, the fabrication procedures were simplified remarkably compared with conventional self-assembly or e-beam lithography processes. We also demonstrate that highly sensitive tuning of PBGs can be achieved by fluidic actuation, which is an essential feature for tunable micro-lasers and optical switches and filters. In addition, the interconnected porous structures in multiple length scales can be used for micro-catalytic reactors and micromixers.

Acknowledgements

This work was supported by a grant from the Creative Research Initiative Program of the Ministry of Science & Technology for "Complementary Hybridization of Optical and Fluidic Devices for Integrated Optofluidic Systems." Partial support from the Brain Korea 21 Program is also appreciated.

Notes and references

1 M. Maldovan, C. K. Ullal, W. C. Carter and E. L. Thomas, *Nat. Mater.*, 2003, **2**, 664.
2 M. D. Malinsky, K. L. Kelly, G. C. Schatz and R. P. Van Duyne, *J. Am. Chem. Soc.*, 2001, **123**, 1471.
3 K. Kneipp, H. Kneipp, I. Itzkan, R. R. Dasari and M. S. Feld, *J. Phys.: Condens. Matter*, 2002, **14**, R597.
4 D. Psaltis, S. R. Quake and C. H. Yang, *Nature*, 2006, **442**, 381.
5 P. Mach, T. Krupenkin, S. Yang and J. A. Rogers, *Appl. Phys. Lett.*, 2002, **81**, 202.
6 J. Hsieh, P. Mach, F. Cattaneo, S. Yang, T. Krupenkine, K. Baldwin and J. A. Rogers, *IEEE Photon. Technol. Lett.*, 2003, **15**, 81.
7 U. Levy, K. Campbell, A. Groisman, S. Mookherjea and Y. Fainman, *Appl. Phys. Lett.*, 2006, **88**, 111107.
8 D. Erickson, T. Rockwood, T. Emery, A. Scherer and D. Psaltis, *Opt. Lett.*, 2006, **31**, 59.
9 G. L. Liu and L. P. Lee, *Appl. Phys. Lett.*, 2005, **87**, 074101.
10 S. -K. Lee, G. -R. Yi and S. -M. Yang, *Lab Chip*, 2006, **6**, 1171.
11 J. H. Moon, J. Ford and S. Yang, *Polym. Adv. Technol.*, 2006, **17**, 83.
12 L. J. Wu, Y. C. Zhong, C. T. Chan, K. S. Wong and G. P. Wang, *Appl. Phys. Lett.*, 2005, **86**, 241102.
13 H. Fudouzi and Y. Xia, *Adv. Mater.*, 2003, **15**, 892.
14 P. Yang, T. Deng, D. Zhao, P. Feng, D. Pine, B. F. Chmelka, G. M. Whitesides and G. D. Stucky, *Science*, 1998, **282**, 2244.
15 Y. J. Zhang, S. P. Wang, M. Eghtedari, M. Motamedi and N. A. Kotov, *Adv. Funct. Mater.*, 2005, **15**, 725.
16 S. Jeon, V. Malyarchuk, J. O. White and J. A. Rogers, *Nano Lett.*, 2005, **5**, 1351.
17 J. H. Moon, A. J. Kim, J. C. Crocker and S. Yang, *Adv. Mater.*, 2007, **19**, 2508.
18 J. H. Moon, W. S. Chang, D. J. Pine and S. -M. Yang, *Appl. Phys. Lett.*, 2004, **85**, 4184.
19 S. -H. Kim, S. Y. Lee, G. -R. Yi, D. J. Pine and S. -M. Yang, *J. Am. Chem. Soc.*, 2006, **128**, 10897.
20 W. A. Murray, S. Astilean and W. L. Barnes, *Phys. Rev. B*, 2004, **69**, 165407.
21 E. Yablonovitch, *J. Phys.: Condens. Matter*, 1993, **5**, 2443.
22 M. H. Wang, D. W. Brandl, F. Le, P. Nordlander and Naomi J. Halas, *Nano Lett.*, 2006, **6**, 827.